Materials Chemistry and Physics 350 (2026) 131871

Contents lists available at ScienceDirect

Materials Chemistry and Physics

journal homepage: www.elsevier.com/locate/matchemphys

Surface plasmon resonance optical sensing of hydrocarbon vapours using a Schiff base–piperazine chemoreceptor

Erkan Halay [a,b,*], Inci Capan [c], Emriye Ay [d], Yaser Acikbas [e], Rifat Capan [c]

[a] Department of Chemistry, Scientific Analysis Technological Application and Research Center, Usak University, Usak, 64200, Turkey
[b] Department of Chemistry and Chemical Processing Technologies, Banaz Vocational School, Usak University, Usak, 64500, Turkey
[c] Department of Physics, Faculty of Arts and Science, University of Balikesir, Balikesir, 10145, Turkey
[d] Department of Chemistry, Faculty of Engineering and Natural Sciences, Manisa Celal Bayar University, Manisa, 45110, Turkey
[e] Department of Electrical and Electronics Engineering, Usak University, Usak, 64200, Turkey

HIGHLIGHTS

- A piperazine-based Schiff base was designed as a potential chemosensor.
- Gas sensing ability toward benzene, ethanol, and acetone vapours was evaluated for the first time.
- Adsorption kinetics were analyzed using the Elovich model for all analyte vapours.
- The thin film SPR sensor demonstrated promising potential for intelligent gas classification and healthcare applications.

GRAPHICAL ABSTRACT

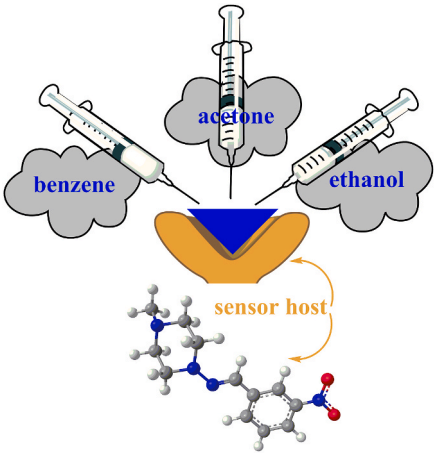

ARTICLE INFO

Keywords:
Schiff base material
Vapour sensor
Surface plasmon resonance
Elovich model

ABSTRACT

Herein, a Schiff base sensor candidate derived from piperazine heterocycle and substituted aromatic group, namely 4-methyl-*N*-(3-nitrobenzylidene)piperazin-1-amine (**NBPA**) was synthesized and thin films of this derivative were examined through surface plasmon resonance technique for its chemoreceptor feature against some organic vapours of distinct character such as benzene, ethanol and acetone. The ranges of some sensor parameter values, including sensitivity (0.0763–0.2675 × 10^{-3} response/ppm), LOD (43.25–12.33 ppm), and LOQ (131.06–37.38 ppm), are presented for the NBPA-based thin film exposed to these organic vapours. Furthermore, the adsorption kinetics of the NBPA thin film when exposed to these vapours at different concentrations were investigated by analysing the experimental SPR data using the Elovich model. For acetone, ethanol, and benzene vapours, the Elovich constant a ranged from 524.19 to 5493.24, 458.47–3734.67, and 598.03–2900.75 ppm/mm^2, respectively, while the corresponding b values were between 0.17 and 0.01, 0.22–0.02, and 0.42–0.02

* Corresponding author. Department of Chemistry, Scientific Analysis Technological Application and Research Center, Usak University, Usak, 64200, Turkey.
E-mail address: erkan.halay@usak.edu.tr (E. Halay).

https://doi.org/10.1016/j.matchemphys.2025.131871
Received 13 August 2025; Received in revised form 10 November 2025; Accepted 30 November 2025
Available online 2 December 2025

mm^2s/ppm. These results indicated that heterocyclic and aromatic moiety aided Schiff base material could be triggered for superior intermolecular interactions, and thus the potential of Schiff bases to reveal sensitive chemoreceptors that will broaden new horizons has been confirmed once again.

1. Introduction

In both developing industries and the groves of academe, the detection of harmful gases like hydrocarbons and volatile organic compounds (VOCs) has been risen in importance due to the growing concerns for healthcare and environmental monitoring [1–3]. Conventional detection of volatile hydrocarbons by the methods based on instrumental techniques including infrared spectroscopy, gas chromatography with specialized detectors (Flame Ionization (FID), Photo Ionization (PID), Thermal Conductivity (TCD) and Mass (MS) Detectors, etc.) has been carried out at present [4–6]. Although these instruments make it suitable for accurate detection and comprehensive scientific research, their high cost, large-sized setup, and the need for time-consuming procedures and professional skills make them inappropriate for real-time detection and analysis [7]. For these reasons, as an alternative approach, chemical sensors which are constructed from organic materials have been widely used due to their unique electronic structures and structural properties [8,9]. Thus, related organic derivatives obtained by modifying their skeleton and/or introducing different substituents into the main skeleton allow researchers to design a variety of sensors for the determination of gaseous analytes [10,11].

These types of existing sensors are mainly based on the basis of electrochemical, optical, acoustic, luminescent, mass-sensitive, conductometric, piezoelectric and thermal signal transduction mechanisms [12–17]. Among them, Surface Plasmon Resonance (SPR) is a technique incorporating optical, highly sensitive sensors that make use of metal film excitation in order to find the presence and concentrations of analytes in various samples [18]. SPR sensors measure a change in the refractive index of this metal film surface which is caused by binding of the analyte to the sensing molecule that is on the metal surface [19]. Çimen et al. [20], in their review, highlight how (Molecularly Imprinted Polymer) MIP-based plasmonic sensors enable the label-free, highly selective and sensitive detection of various environmental contaminants. This is achieved by integrating nanomaterials and plasmonic transduction layers. Moreover, recent studies [21,22] have demonstrated the MIP method's effectiveness in various sensing applications. This further validates its versatility and robustness when used with diverse analytes, ranging from small molecules to biomacromolecules.

By measuring the relevant change, a broad range of gaseous species and VOCs including the recognized candidates as the most noteworthy ones like benzene, ethanol and acetone can be qualitatively and/or quantitatively detected [23–27]. This can be attributed to the fast growing of industrialization and the expansion of laboratory/medical applications, as the emissions of these VOCs pose a significant threat to human health and have therefore attracted considerable public attention. Among these VOCs, for instance, acetone has emerged as a non-invasive biomarker (breath acetone, BrAce) present in the exhaled breath of both healthy and diabetic individuals. Its concentration correlates with metabolic alterations associated with diabetes, motivating intense development of highly sensitive VOC sensors for healthcare monitoring [28]. The same sensing mechanisms and engineered materials are also relevant to industrial applications, where acetone leakage poses significant environmental and safety concerns [29,30]. Accordingly, in order to meet the demands in this field and overcome the challenges in the design of gas sensors, much research has been dedicated to exploration of various organic molecules as sensing candidates [31].

While important steps have been taken for the preparation of gas sensors based on various materials ranging from organic-based compounds to metal-based materials [32–37], it is clear that the sensing performance is closely related to the structure and composition [38], and in this regard, Schiff bases present unique feature in view of its components and the imine bond along with electronic configurations [39–41]. In contrast to previous reports in the literature, this study focuses on a Schiff base analogue designed to exhibit coordination capability through diverse weak interactions with various molecular species, and which can be derivatized with different organic building blocks due to its stabilizing effects on electronic configuration and therefore intermolecular interactions. These characteristics distinguish it from conventional sensor materials in terms of selectivity and sensitivity, and hence as a potential sensor candidate, the Schiff base derivative consisting of piperazine and nitro-substituted units was systematically investigated for its gas sensing behaviour toward benzene, ethanol and acetone vapours. Moreover, to the best of our knowledge, although Schiff base-based sensors have been effectively employed for the detection of ionic species (e.g., H^+) in aqueous media, and molecular gases like NH_3 and HCl, their use in sensing volatile organic compounds including ethanol, benzene, and acetone has not yet been explored.

In the light of aforementioned information given in detail above, this paper aspires to be a space-filler in the exploration of Schiff base-based sensors offering considerable occasions thanks to their functional groups and distinct electronic properties which enhance their gas sensing capabilities, particularly in the context of Schiff bases detecting VOCs.

2. Experimental section

2.1. Preparation of NBPA chemosensor thin film

The synthetic procedure and spectroscopic characterization of this sensor compound **NBPA** are given in the Supplementary Material (Figs. S1–S5). The spectroscopic characterization data are consistent with those previously reported in the literature [42]. In Fig. 1, the chemical structure of the **NBPA** molecule is shown, which is investigated as a potential chemical sensor in thin-film material form.

2.2. Gas measurement technique

The gas sensing characterization was performed with the SPR setup, Biosuplar 6 model SPR system with a He–Ne laser (632.8 nm) and an angular resolution of 0.003°. A glass prism was mounted onto a holder to provide the Kretschman configuration to generate the surface plasmons. The p-polarized beam is totally internal reflected when directed above the critical angle. At a special angle θ_{SPR} the SPR formation is supplied between the interface gold/thin film (metal/dielectric) via their negatively signed dielectric constants, exciting the delocalized electrons of the gold layer, bringing them into resonance. Therefore, the reflected light intensity experiences a dramatic decrease at the θ_{SPR}. For the gas sensing experiments benzene, acetone, ethanol with a purity of 99 % (Sigma-Aldrich) were used without further purification. The saturated vapours were supplied by filling the half volume of a glass flask with the liquid form of the volatile solvents in room temperature; therefore, the saturated vapour will fulfil the other half. The saturated form of each VOC was transferred into a 1 mL injector to expose it into the gas cell. The gas sensing measurements were performed in 5 steps; 0.2 mL of saturated vapour was mixed with dry air to reach the volume of 1 mL where in each step the saturated vapour volume is increased as 0.4 mL, 0.6 mL, 0.8 mL and the rest of the volume was completed with dry air. In the last step 1 mL of the volume was fulfilled with saturated vapour only. The exposures of the vapour and flushing with the dry air lasted for 2 min, each periodically. The reciprocal exposures of the saturated vapour

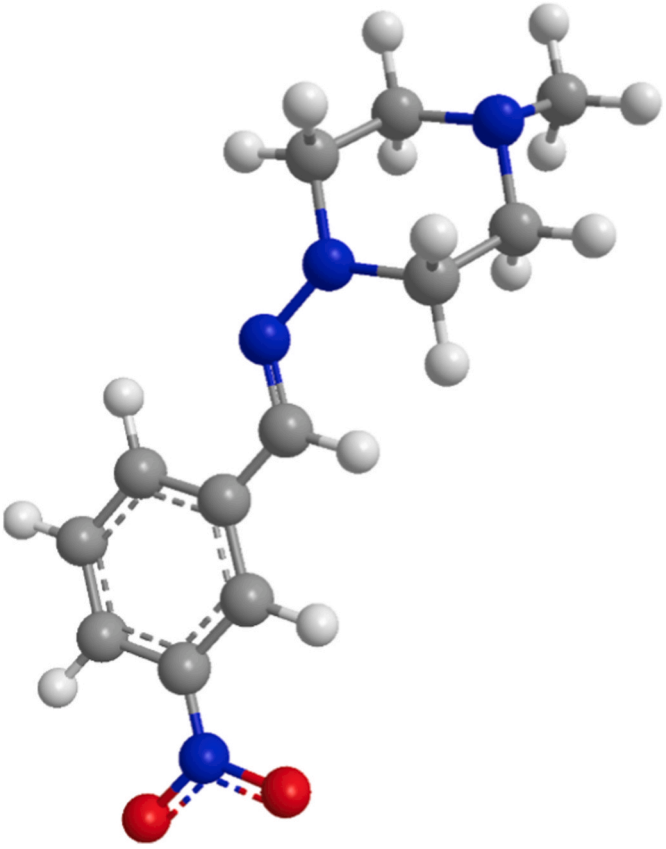

Fig. 1. 3-Dimension Molecular Structure (ball-and-stick model) of NBPA sensor candidate.

were used to monitor the reproducibility of the **NBPA** thin film sensors. All measurements were repeated three times at room temperature (20 °C) and the relative humidity (RH) value was 25 % which is monitored by HTC-2 LCD Digital Thermometer Hygrometer. The SPR-gas measurement system is given in Fig. 2.

2.3. Theoretical model

In gas sensor applications, the study of adsorption dynamics is important in terms of investigating the surface adsorption, diffusion and desorption interactions between the sensitive sensor material and the selected gas molecule to be detected. These interactions are highly dependent on the physical and chemical properties of applied gas. Several models such as Pseudo, Elovich, Langmuir adsorption models etc. have been developed to analyse the obtained experimental data. The piperazine-based Schiff base SPR sensor chip, which was previously prepared using this Schiff base material, was exposed to organic vapours containing chlorine compounds and their adsorption dynamics were analyzed using the Elovich model [42]. In this study, the same SPR sensor chip was used to investigate the sensor properties and adsorption dynamics against acetone, ethanol, and benzene vapours. The experimental results obtained for these vapours will be analyzed using the Elovich model which allows us to determine the adsorption efficiency, the rate of adsorption, the suitability of fitting parameters and the correlation coefficient [43,44].

The Elovich model is based on two assumptions: the amount of activation energy increases with adsorption time, and the adsorbent surface is heterogeneous [45]. Therefore, the Elovich model is suitable to analyse the data recorded from a solid film during the interaction between a solid surface and adsorbents. The adsorption capacity (the adsorption amount per unit area), q_t, for a time-dependent SPR kinetic measurement is described as [46]:

$$q_t = \left[\frac{(I_i - I_e)V}{A}\right] \quad \text{(Eq. 1)}$$

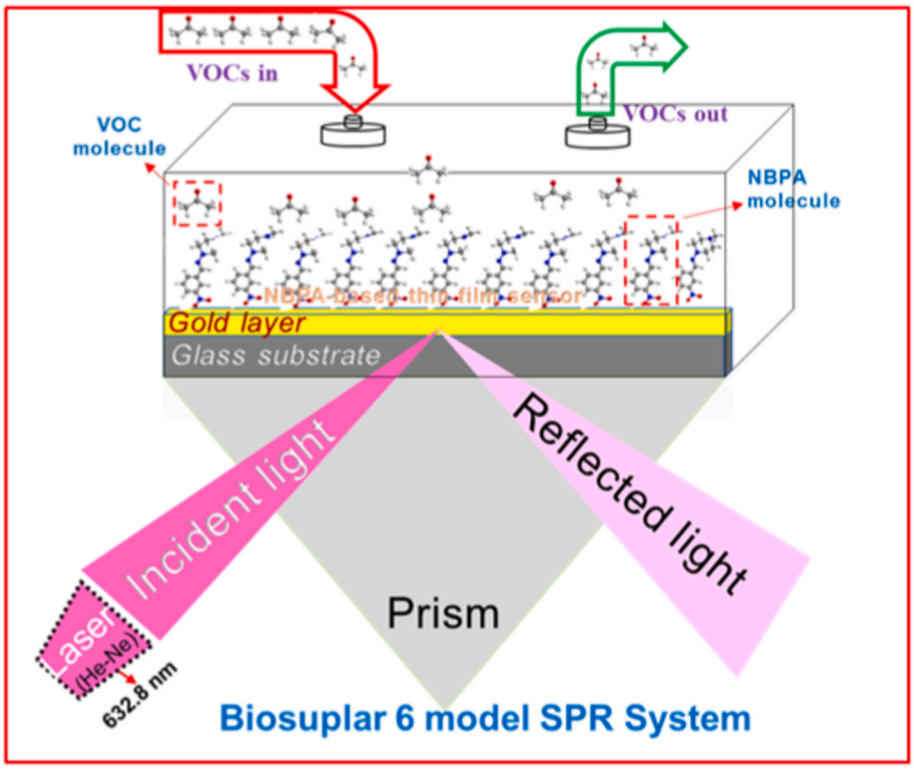

Fig. 2. SPR-gas measurement system.

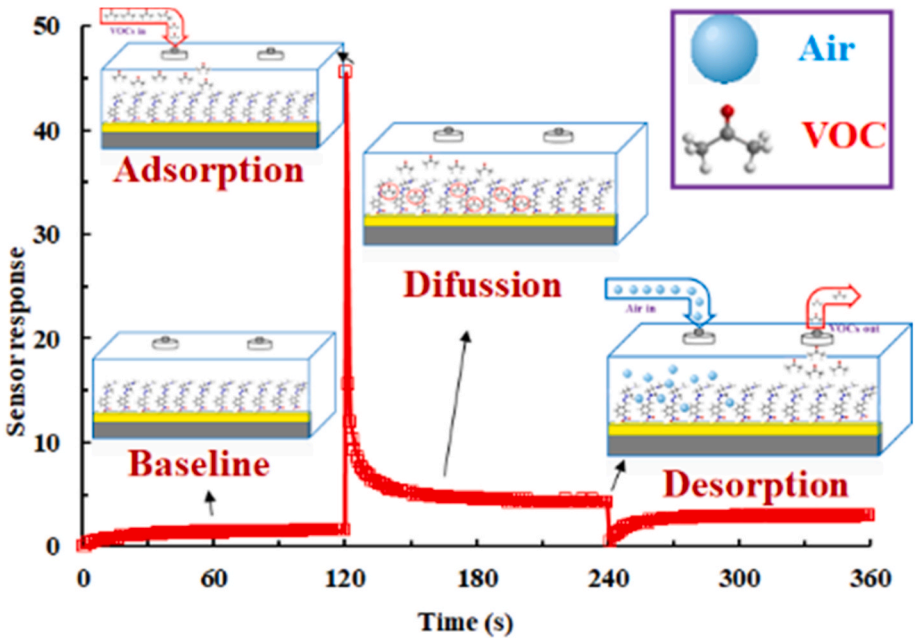

Fig. 3. A schematic diagram of the SPR sensing mechanism.

where I_i is the initial reflected light intensity value, I_e is the equilibrium reflected light intensity value, V is the volume of the injected vapour and A is the surface area of thin film respectively.

The adsorption rate as a function of time (dq_t/dt) for the Elovich model is given as [47]:

$$\frac{dq_t}{dt} = a \exp(-b\, q_t) \qquad \text{(Eq. 2)}$$

where a is the initial adsorption rate, q_t is the quantity of gas adsorbed at time t and b is the Elovich desorption constant respectively.

If q_t is chosen as 0, Eq. (2) is equal to a value which is regarded as the initial adsorption rate. If the boundary conditions can be chosen from $q_t = 0$ at t = 0 and $q_t = q_t$ at t = t, Eq. (2) can be integrated as [48]:

$$q_t = \left(\frac{1}{b}\right)\ln(ab) + \left(\frac{1}{b}\right)\ln(t) \qquad \text{(Eq. 3)}$$

Eq. (3) can be applied to the experimental data for a calculation of a and b values which are used to understand the nature of gas adsorption onto a thin film.

If $t \gg t_0$ is assumed that the validity of Eq. (3) can be checked by plotting q_t versus *lnt* which yields a linear relationship. Using the intercept $\left(\frac{1}{b}\right)lnab$ and the slope $\left(\frac{1}{b}\right)$ of this relationship the a and b values can be determined [49]. The correlation coefficient (R^2) of this graph gives us an indicator of the conformity between SPR experimental data and the Elovich model parameters.

3. Results and discussion

3.1. Characterization of the NBPA thin films

The nanometric morphology of **NBPA** thin films was examined using atomic force microscopy (AFM) and scanning electron microscopy (SEM) techniques. Fig. S6a and S6b show the 2D and 3D topographical images of the film surface on a glass substrate. Image analysis of a 10 × 10 μm μm scan area revealed roughness and RMS area values of 2.09 and 2.84 nm, respectively. While some regions have relatively high surface peaks, the film's overall surface appears homogeneous and smooth. Additionally, the SEM image shown in Fig. S7 revealed that the NBPA-coated glass surface had a uniform morphology, suggesting that NBPA molecules were distributed evenly across the surface.

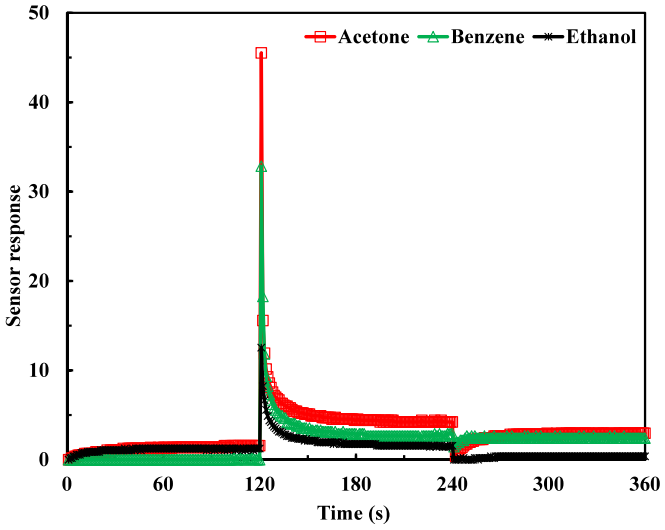

Fig. 4. The kinetic response of **NBPA**-based SPR sensor.

3.2. Sensor parameters of NBPA thin film sensor

The interactions of **NBPA** thin films with volatile organic vapours were investigated using the spin coating production technique on a gold-coated glass substrate. Kinetic interactions of the **NBPA** thin films with benzene, acetone, and ethanol vapours were studied using the SPR method.

Generally, the sensing mechanism (given in Fig. 3) can be performed in four steps (baseline, adsorption, diffusion, and desorption). In the early baseline, **NBPA**-based thin film sensor exposed to dry air for 120 s and in this period of time, the response was a stable. The initial response of the **NBPA** -based thin film sensor showed a sharp increase for all harmful organic vapours between 120 and 125 s due to the surface adsorption effect. Once the vapour molecules have been transported into

Table 1
Some physical properties of vapours.

Vapours	Molecular weight (g mol^{-1})	Vapour pressure (kPa)	Sensor response (ΔI/Io × 100)
Benzene	78.11	9.95	32.85
Acetone	58.08	30.6	45.52
Ethanol	46.11	5.95	12.54

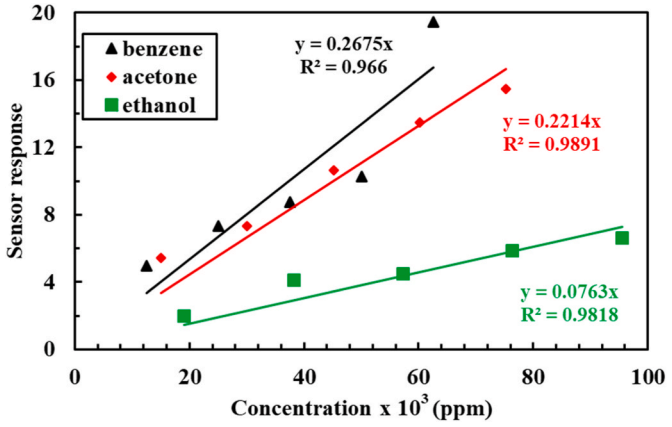

Fig. 5. The response of **NBPA**-based SPR sensor against to three different VOCs at different concentrations.

the **NBPA**-based thin film, the bulk diffusion effect takes over, and the response decreases exponentially. At 240 s, the response to dry air decreased instantaneously, followed by a recovery process (between 240 and 244 s) for all harmful organic vapours due to desorption of the vapours. The response of the **NBPA**-based thin film sensor is stable after 245 s, and the sensor returns to the initial baseline.

Fig. 4 shows the kinetic studies of the **NBPA**-based SPR sensors' interaction with three different vapours. The response is presented in terms of the

$$Sensor\ response = \left(\frac{\Delta I}{I_0}\right) x\ 100 \qquad \text{(Eq. 4)}$$

where ΔI describes the difference in the reflected light intensity before the interaction between the thin film and vapour molecules (I_o) and after exposure to selected vapour molecules (I). From Fig. 4, it can be seen that the reflected light intensity was kept constant for the first 120 s of the time-dependent response measurements. Then, selected vapour was injected into the gas cell at the 120th second, after which the amount of reflected light intensity was recorded for the following 120 s. After 240 s, fresh air was injected into the gas cell to clean it of volatile organic vapour. A similar process was carried out for kinetic study by exposing the NBPA thin film to acetone, ethanol, and benzene vapours at five different concentrations, as shown in Fig. 6a, 7a and 8a, respectively.

The three different vapour response values of the NBPA thin film can be explained by the physical parameters of the VOCs presented in Table 1. Among the organic vapours tested, the **NBPA** thin film sensor exhibited the highest response to acetone vapour ($\Delta I/I_o \times 100$). This may be due to acetone having higher vapour pressure compared to other vapours. The rapid change in response is believed to be directly

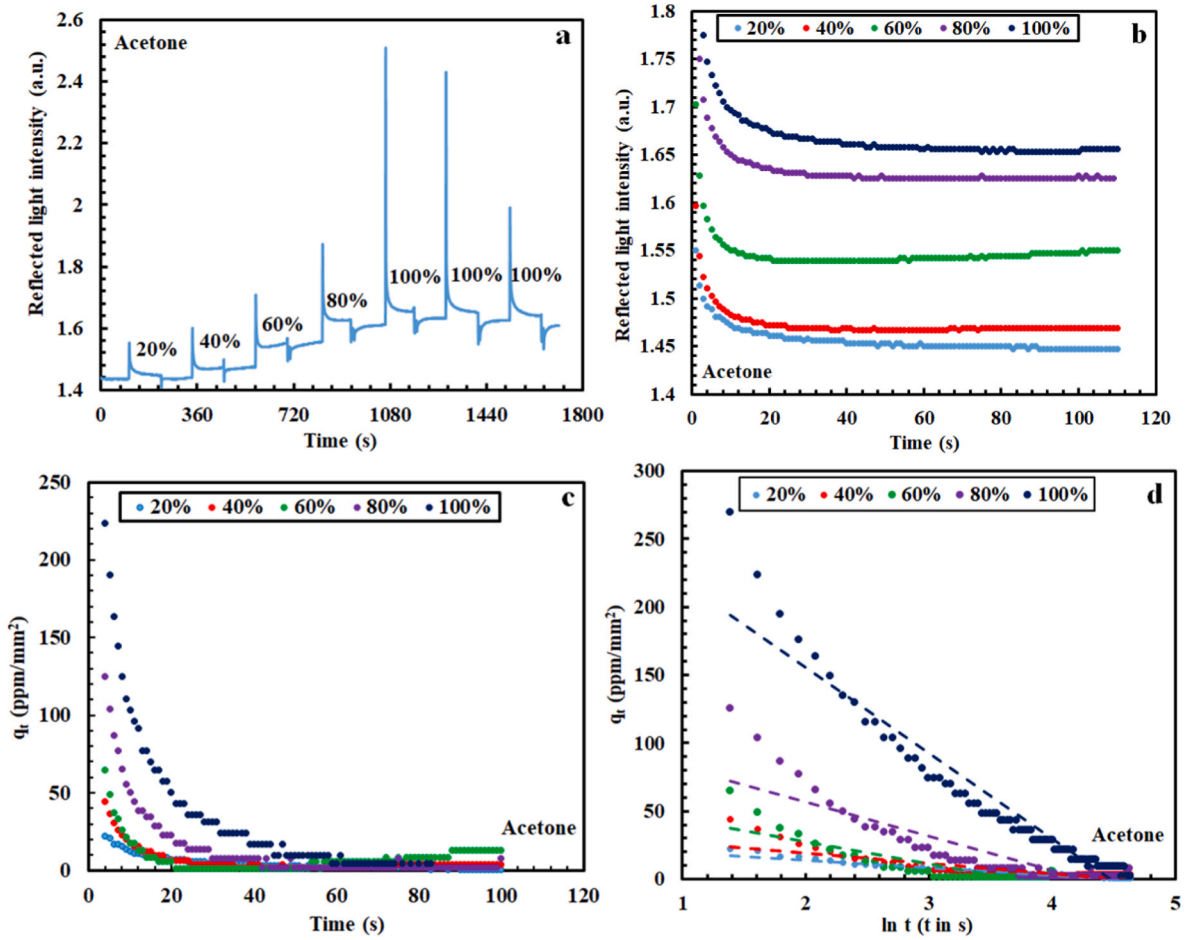

Fig. 6. Adsorption results of **NBPA** thin film for acetone vapour.

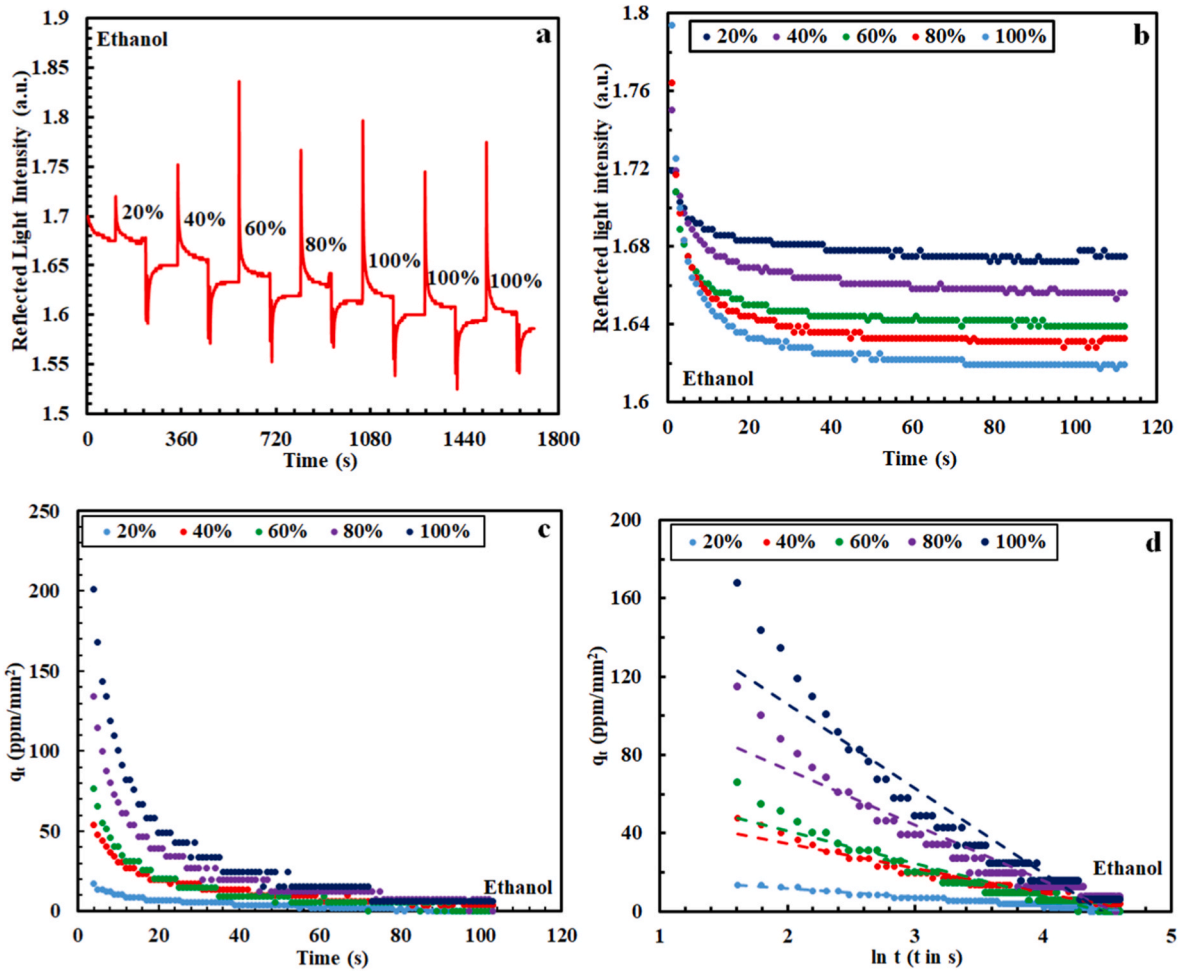

Fig. 7. Adsorption results of **NBPA** thin film for ethanol vapour.

proportional to the vapour pressure value once the vapour is released into the gas cell.

The kinetic measurements were analyzed through the sensor parameters such as sensitivity (S), limit of detection (LOD), limit of quantification (LOQ), response and recovery times.

Sensitivity was calculated as

$$S = \frac{Sensor\ response}{c} \quad \text{(Eq. 5)}$$

in terms of ppm^{-1} which represents the response per unit concentration of vapour molecules. Concentration dependence calibration curves of **NBPA** thin film are given in Fig. 5. The calibration curves are generated for this purpose that present the linear relation between the response with increasing concentration of each vapour. The S values are calculated using this linear relationship and are listed in Table 2. The highest S value is obtained for benzene vapour and the lowest S value for ethanol vapour.

LOD value of a sensor material describes the lowest amount of the selected vapour that can be detected. LOQ value is known as the lowest amount of the selected vapour that can be accurately quantified. These two important sensor parameters indicate a higher sensitivity and precision of a sensor material. The LOD [50] and the LOQ [51] values can be given as:

$$LOD = \frac{3.3\,\sigma}{S} \quad \text{(Eq. 6)}$$

$$LOQ = \frac{10\,\sigma}{S} \quad \text{(Eq. 7)}$$

where σ is the standard deviation for our SPR measurements (0.001) and S is the sensitivity of **NBPA** thin film.

For comparative performance metrics, a comprehensive study using different thin films is summarized in Table 3.

In this study, the responses of **NBPA** thin films to three different organic vapours were recorded using SPR kinetic measurements. These response data and the calculated sensor parameters are shown in Tables 1 and 2. Physical property parameters such as vapour pressure, dipole moment and molecular weight of the vapours tested can explain the measured and calculated sensor parameter values (response, sensitivity, LOD, LOQ, response and recovery times) for the **NBPA** thin film sensor [60,61].

The overall sensitivity for the NBPA-based SPR sensor is in the following order: benzene > acetone > ethanol. This can be explained by considering the molecular weights. The order of sensitivity is the same as the molecular weight of the vapours: benzene (78.11 g mol^{-1}), acetone (58.08 g mol^{-1}) and ethanol (46.11 g mol^{-1}). A larger vapour molecular weight leads to higher sensitivity, which aligns well with previous findings in the literature [62–64]. When the number of molecules that can be adsorbed by an adsorbent is limited, it is reasonable to assume that a larger molecular weight of the adsorbent will lead to greater sensitivity.

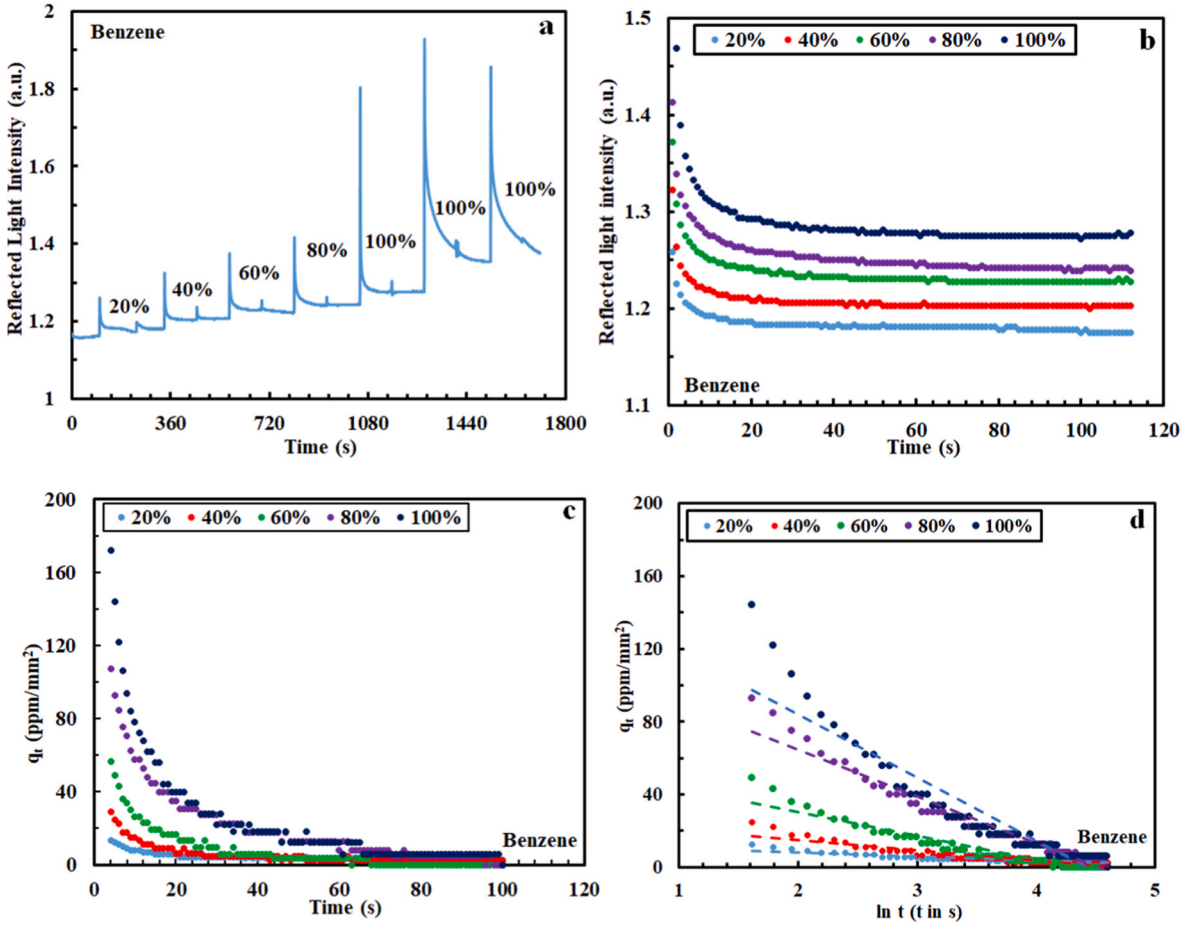

Fig. 8. Adsorption results of **NBPA** thin film for benzene vapour.

Table 2
Sensor parameters for the NBPA thin-film sensor.

VOCs	Sensitivity (Response/ ppm) x 10^{-3}	LOD (ppm)	LOQ (ppm)	Response/ Recovery times (s)
Benzene	0.2675	12.33	37.38	2/5
Acetone	0.2214	14.90	45.17	2/7
Ethanol	0.0763	43.25	131.06	2/5

3.3. Adsorption results of NBPA thin film

The Elovich constants (*a* and *b*) and R^2 parameters for the Elovich model versus each concentration value were calculated using the time-dependent SPR kinetic measurement data for acetone, ethanol, and benzene vapours of the **NBPA** thin film given in Figs. 6–8, respectively, as well as Eqs. (1) and (3). These values are given in Table 4. An understanding of the adsorption behavior was obtained by collecting the values of reflected light intensity for each concentration from Fig. 6a, 7a and 8a. These values were recorded while the vapour molecules were exposed to the gas cell until dry air was introduced.

The selected data on the intensity of reflected light for acetone, ethanol, and benzene vapours as a function of time is shown in Fig. 6b, 7b and 8b, respectively. The q_e values of the thin film sensor **NBPA** were determined with the help of Eq. (1) and are presented in Fig. 6c, 7c and 8c for acetone, ethanol, and benzene vapours, respectively. Eq. (3) and Fig. 6d, 7d and 8d are used for Elovich model to determine *a* and *b* constants which are given in Table 4.

It is clear that the values for all three vapours increase while *b* values decrease depending on the concentration. As the concentration value increases, *a* value also increases rapidly because the interaction between vapour molecules and **NBPA** thin film sensors increases rapidly when the vapour molecules are adsorbed. The *b* value shows a rapid decrease due to the desorption process slower with the increase in the concentration amount.

Table 4 shows the Elovich constants (*a* and *b*) that were calculated for the different concentrations of the three vapours to which the SPR-based **NBPA** sensor was exposed. The Elovich constant, *a*, was found to be in the range of 524.19–5493.24 ppm/mm^2 for acetone vapour, 458.47–3734.67 ppm/mm^2 for ethanol, and 598.03–2900.75 ppm/mm^2 for benzene vapour at different concentrations. The other Elovich constant (*b*) was calculated to be in the range of 0.17–0.01, 0.22–0.02, and 0.42–0.02 mm^{2}s/ppm for acetone, ethanol, and benzene vapours, respectively. The Elovich constant (*a*) of acetone vapour at saturated concentration is higher than that of other vapours. The result obtained can be attributed to acetone's high vapour pressure and dipole moment compared to the other vapours. This result may be due to dipole-dipole interactions between the adsorbed vapour molecules and the thin film material. The order of Elovich constants at saturated concentrations for three different vapours is the same as the order of their dipole moment values (acetone (2.91 D) > ethanol (1.69 D) > benzene (0 D)).

In order to analyse a sensor interaction, the adsorption process between the thin film and target adsorbent is another sensing interaction factor that must be investigated. In an adsorption feature, the adsorbate encounters the surface, interacts with the surface, and then migrates into the film structure [65]. The chemical and physical interactions between the gas molecules (analyte) and the thin film (adsorption agent) occur, in which the pore volume and size distribution of the surface, molecular weight, polarity, saturated vapour pressure of the gas molecules, and

Table 3
The existing sensors for selected vapours.

Thin film sensor	Test technique	Tested vapour	***S***	***LOD*** (ppm)	***LOQ*** (ppm)	Refs
The **nanofiber sensor** PAN-RHE	Quartz Crystal Microbalance (QCM)	acetone	0.0243 Hz/ppm	135.80	411.52	[52]
		ethanol	0.0091 Hz/ppm	362.63	1098.9	
		benzene	No good response	–	–	
Metal organic framework (MOF) MIL-101(Cr)		acetone	0.090 Hz/ppm	no report	no report	[53]
		ethanol	0.450 Hz/ppm			
N-cyclohexylmethacrylamide LB thin films		acetone	0.044 Hz/ppm	67.72	no report	[54]
		ethanol	0.029 Hz/ppm	100.33		
		benzene	0.047 Hz/ppm	63.83		
Tetranitro-oxacalix [4]arenes thin film	SPR	acetone	0.0700 response/ppm	no report	no report	[55]
		ethanol	0.0166 response/ppm			
		benzene	0.0400 response/ppm			
Pyridine modified calix [4]arene Langmuir-Blodgett thin film sensor		acetone	0.477 response/ppm	7.79×10^3	no report	[56]
		benzene	0.185 response/ppm	6.52×10^3		
TiO_2 thin film sensing layer		ethanol	1.13×10^{-6} (1/ppm)	22×10^3	no report	[57]
HKUST-1 metal–organic framework (MOF) via a layer-by-layer		acetone	13.7 nm/%	0.005 %	no report	[58]
		ethanol	15.5 nm/%	0.003 %		
Chitosan-polyethylene glycol (PEG)-based surface plasmon resonance (SPR) sensor		acetone	0.348°/ppm	5	no report	[59]
4-methyl-*N*-(3-nitrobenzylidene)piperazin-1-amine (**NBPA**) thin film		dichloromethane	1.78 response/ppm	1.85	5.62	[42]
		chloroform	2.27 response/ppm	1.45	1.94	
		trichloroethylene	1.70 response/ppm	1.94	5.88	
		acetone	0.2675×10^{-3} response/ppm	12.33	37.38	This work
		ethanol	0.2214×10^{-3} response/ppm	14.90	45.17	
		benzene	0.0763×10^{-3} response/ppm	43.25	131.06	

Table 4
Adsorption results of NBPA thin film for three different organic vapours.

Organic vapour	C (%)	Fitting equation	R^2	Elovich constant	
				a (ppm/mm^2)	b (mm^2s/ppm)
Acetone	20	y = −5.5832x + 25.36	0.9369	524.1938	0.1791
	40	y = −7.4709x + 33.922	0.6392	701.4256	0.1338
	60	y = −17.124x + 62.095	0.721	643.8346	0.0613
	80	y = −25.031x + 106.63	0.7638	1772.267	0.0399
	100	y = −62.839x + 280.94	0.7638	5493.247	0.0159
Ethanol	20	y = −4.4115x + 20.486	0.9657	458.4788	0.2266
	40	y = −12.539x + 59.623	0.9533	1456.568	0.0797
	60	y = −16.643x + 74.643	0.9059	1475.702	0.0600
	80	y = −28.341x + 129.16	0.9067	2701.626	0.03528
	100	y = −43.005x + 191.98	0.9128	3734.675	0.0232
Benzene	20	y = −2.34x + 12.972	0.8475	598.0359	0.4273
	40	y = −5.553x + 25.898	0.8403	588.7713	0.1800
	60	y = −13.051x + 56.243	0.913	970.9396	0.0766
	80	y = −25.616x + 115.78	0.9536	2351.989	0.0390
	100	y = −34.53x + 153	0.8822	2900.758	0.0289

external conditions can all play an important role within the adsorption process [66]. To understand the sensing mechanism, the different models are applied to the experimental data because the nature of the adsorption interactions between gas molecules and a sensing material is an important issue to develop and optimize high-quality sensors in several areas of application [66–68].

Our earlier report showed that sensing results for different VOCs, such as dichloromethane, chloroform, and trichloroethylene, are higher than acetone, ethanol, and benzene vapours. In addition, the fitting parameters of sensing data using the Elovich model are much better than the current study. These results can be concluded that the NBPA thin film sensor is more sensitive and selective to dichloromethane, chloroform, trichloroethylene vapours than acetone, ethanol, and benzene vapours due to adsorption features.

4. Conclusions

In this study, our piperazine conjugated Schiff base chemoreceptor was, for the first time, employed to broaden its sensing capabilities toward gaseous guest molecules including benzene, ethanol, and acetone, considering their intrinsic physicochemical properties. In related gas sensing experiments, the LOD, LOQ, and sensitivity values were determined to be 43.25–12.33 ppm, 131.06–37.38 ppm, and 0.0763–0.2675 $\times 10^{-3}$ response/ppm, respectively, for the Schiff base-based thin film sensor exposed to organic vapours of different characteristics, namely benzene, ethanol, and acetone. The adsorption kinetics of the NBPA-based SPR optical sensor during the interaction process with this vapour were also discussed, and the results were presented. The adsorption kinetics were studied by calculating the Elovich constants (a and b) using data obtained by exposing the NBPA-based SPR sensor to organic vapours at five different concentrations. The Elovich constant a was calculated to be in the range of 524.19–5493.24, 458.47–3734.67,

and 598.03–2900.75 ppm/mm^2 for the different acetone, ethanol, and benzene vapour concentrations, respectively. Similar calculations were performed for Elovich constant b and were found to be in the range of 0.17–0.01, 0.22–0.02, and 0.42–0.02 mm^{2}s/ppm for acetone, ethanol, and benzene vapours, respectively. In light of these findings, Schiff base host molecule modified with a piperazine heterocyclic core has emerged as a promising candidate for developing high-performance sensors targeting gaseous guest analytes, including benzene, ethanol, and acetone, with potential applications in medicine and healthcare. To enhance the selectivity of the related host molecule, our study also incorporated detailed investigations aimed at gas classification. Consequently, this study lays a solid foundation for the selective recognition capabilities of intelligent gas sensing technologies.

CRediT authorship contribution statement

Erkan Halay: Writing – review & editing, Writing – original draft, Methodology. **Inci Capan:** Writing – review & editing, Methodology, Formal analysis, Conceptualization. **Emriye Ay:** Validation, Methodology, Investigation. **Yaser Acikbas:** Writing – review & editing, Writing – original draft, Supervision, Data curation. **Rifat Capan:** Writing – review & editing, Data curation, Conceptualization.

Declaration of competing interest

The authors declare that they have no known competing financial interests or personal relationships that could have appeared to influence the work reported in this paper.

Acknowledgements

Support and assistance provided by UBATAM (Usak University Scientific Analysis Technological Application and Research Center) are gratefully acknowledged.

Appendix A. Supplementary data

Supplementary data to this article can be found online at https://doi.org/10.1016/j.matchemphys.2025.131871.

Data availability

Data will be made available on request.

References

[1] M.S.A.B. Shakin, M.T. Rahman, S.N. Shanto, M.M. Rana, Au-loaded WS_2/SnO_2 heterostructure for room temperature detection of CO at ppb-level, IEEE Sens. J. 24 (2024) 36386–36392, https://doi.org/10.1109/JSEN.2024.3467052.
[2] S. Acharyya, S. Nag, S. Kimbahune, A. Ghose, A. Pal, P.K. Guha, Selective discrimination of VOCs applying gas sensing kinetic analysis over a metal oxide-based chemiresistive gas sensor, ACS Sens. 6 (2021) 2218–2224, https://doi.org/10.1021/acssensors.1c00115.
[3] M. Poloju, N. Jayababu, E. Manikandan, M.V.R. Reddy, Enhancement of the isopropanol gas sensing performance of SnO_2/ZnO core/shell nanocomposites, J. Mater. Chem. C 5 (2017) 2662–2668, https://doi.org/10.1039/c6tc05095f.
[4] M. Zhou, X. Li, Q. Wang, In situ growth of nanorod-assembled $SnWO_4$ via AACVD for ppb level xylene gas sensor, J. Electron. Mater. 54 (2025) 348–360, https://doi.org/10.1007/s11664-024-11609-5.
[5] V. Amiri, H. Roshan, A. Mirzaei, G. Neri, A.I. Ayesh, Nanostructured metal oxide-based acetone gas sensors: a review, Sensors 20 (2020) 3096, https://doi.org/10.3390/s20113096.
[6] Y.M. Lim, V. Swamy, N. Ramakrishnan, E.S. Chan, H.P. Kesuma, Volatile organic compounds (VOCs) in wastewater: recent advances in detection and quantification, Microchem. J. 195 (2023) 109537, https://doi.org/10.1016/j.microc.2023.109537.
[7] A. Das, R. Manjunatha, K.N. Kumar, D. De, R. Bandyopadhyay, Fabrication of surface functionalized QCM sensor for BTX detection at ambient conditions, Talanta 283 (2025) 127081, https://doi.org/10.1016/j.talanta.2024.127081.
[8] Q. Lin, C. Zhao, M. Li, H. Xu, Recent progress in surface acoustic wave sensors based on low-dimensional materials and their applications, Chemosensors 12 (2024) 255, https://doi.org/10.3390/chemosensors12120255.
[9] X. Peng, X. Wu, M. Zhang, H. Yuan, Metal−organic framework coated devices for gas sensing, ACS Sens. 8 (2023) 2471–2492, https://doi.org/10.1021/acssensors.3c00362.
[10] T. Basova, Phthalocyanine and porphyrin derivatives and their hybrid materials in optical sensors based on the phenomenon of surface plasmon resonance, Chemosensors 12 (2024) 56, https://doi.org/10.3390/chemosensors12040056.
[11] S.K. Rajput, V.S. Mothika, Powders to thin films: advances in conjugated microporous polymer chemical sensors, Macromol. Rapid Commun. 45 (2024) 2300730, https://doi.org/10.1002/marc.202300730.
[12] T. Richard, S. Climensa, Chemical sensors: from fundamentals to the future a review, Adv. Anal. Sci. 5 (2024) 2838, https://doi.org/10.54517/aas.v5i2.2838.
[13] P. Paulraj, A. Manikandan, E. Manikandan, K. Pandian, M.K. Moodley, K. Roro, K. Murugan, Solid-state synthesis of POPD@AgNPs nanocomposites for electrochemical sensors, J. Nanosci. Nanotechnol. 18 (2018) 3991–3999, https://doi.org/10.1166/jnn.2018.15219.
[14] P. Paulraj, A. Umar, K. Rajendran, A. Manikandan, R. Kumar, E. Manikandan, K. Pandian, M.H. Mahnashi, M.A. Alsaiari, A.A. Ibrahim, N. Bouropoulos, S. Baskoutas, Solid-state synthesis of Ag-doped PANI nanocomposites for their end-use as an electrochemical sensor for hydrogen peroxide and dopamine, Electrochim. Acta 363 (2020) 137158, https://doi.org/10.1016/j.electacta.2020.137158.
[15] K. Lokesh, G. Kavitha, E. Manikandan, G.K. Mani, K. Kaviyarasu, J.B.B. Rayappan, R. Ladchumananandasivam, J.S. Aanand, M. Jayachandran, M. Maaza, Effective ammonia detection using n-ZnO/p-NiO heterostructured nanofibers, IEEE Sens. J. 16 (2016) 2477–2483, https://doi.org/10.1109/JSEN.2016.2517085.
[16] M. Shellaiah, K.-W. Sun, K. Anandan, A. Murugan, V. Venkatachalam, M. Bhushan, M. Sivakumar, E. Manikandan, K. Kaliaperumal, W.-T. Li, Luminescent pyrene-derivatives for Hg^{2+} and explosive detection, Chemosensors 13 (2025) 145, https://doi.org/10.3390/chemosensors13040145.
[17] V. Saasa, M. Mokwena, B. Dhonge, E. Manikandan, J. Kennedy, P.P. Murmu, J. Dewar, R. Erasmus, M.F. Whaley, E. Mukwevho, B. Mwakikunga, Optical and structural properties of multi-wall-carbonnanotube-modified ZnO synthesized at varying substrate temperatures for highly efficient light sensing devices, Sens. Transducers J. 195 (2015) 9–17.
[18] R. Gaur, H.M. Padhy, M. Elayaperumal, Surface plasmon assisted toxic chemical NO_2 gas sensor by Au/ZnO functional thin films, J. Sens. Sens. Syst. 10 (2021) 163–169, https://doi.org/10.5194/jsss-10-163-2021.
[19] V. Kumar, S.K. Raghuwanshi, S. Kumar, Recent advances in carbon nanomaterials based SPR sensor for biomolecules and gas detection-A review, IEEE Sens. J. 22 (2022) 15661–15672, https://doi.org/10.1109/JSEN.2022.3191042.
[20] D. Çimen, N. Bereli, A. Denizli, Advanced plasmonic nanosensors for monitoring of environmental pollutants, Curr. Anal. Chem. 19 (2023) e180622206156, https://doi.org/10.2174/1573411018666220618155324.
[21] J. Liang, Y. Li, Y. Wang, Y. Li, X. Liu, Measurement of alkali metal vapor number density based on surface plasmon resonance, IEEE Photonics Technol. Lett. 37 (2025) 757–760, https://doi.org/10.1109/LPT.2025.3566554.
[22] A. Pal, G. Ansari, N. Ahamad, R.B. Yadav, M. Akkur, S. Kumar, S.K. Shah, I. Arora, H. Singh, A. Uniyal, Nitrogen dioxide gas sensing using surface plasmon resonance sensor, Mod. Phys. Lett. B 39 (2025) 2550221, https://doi.org/10.1142/S0217984925502215.
[23] W. Zhang, X. Lang, X. Liu, G. Li, R. Singh, B. Zhang, S. Kumar, Advances in tapered optical fiber sensor structures: from conventional to novel and emerging, Biosensors 13 (2023) 644, https://doi.org/10.3390/bios13060644.
[24] J. Fang, W. Wang, Y. Fan, H. Guan, Q. Wang, D. Liu, R. Xu, S. Ruan, Tin oxide nanoparticles anchored on ordered mesoporous carbon for efficient acetone sensing, Sens. Actuators, B 425 (2025) 136957, https://doi.org/10.1016/j.snb.2024.136957.
[25] Z. Li, W. Zeng, Q. Li, SnO_2 as a gas sensor in detection of volatile organic compounds: a review, Sens. Actuators, A A. 346 (2022) 113845, https://doi.org/10.1016/j.sna.2022.113845.
[26] R.K. Mishra, V. Kumar, L.G. Trung, G.J. Choi, J.W. Ryu, R. Bhardwaj, P. Kumar, J. Singh, S.H. Lee, J.S. Gwag, Recent advances in ZnO nanostructure as a gas-sensing element for an acetone sensor: a short review, Luminescence 38 (2023) 1087–1101, https://doi.org/10.1002/bio.4413.
[27] T. Dunker, A.M. Ferber, H. Sagberg, K.A.H. Bakke, Critical review of potential technologies for a wearable benzene sensor system, Sens. Acutators Rep. 8 (2024) 100210, https://doi.org/10.1016/j.snr.2024.100210.
[28] H. Dong, L. Qian, Y. Cui, X. Zheng, C. Cheng, Q. Cao, F. Xu, J. Wang, X. Chen, D. Wang, Online accurate detection of breath acetone using metal oxide semiconductor gas sensor and diffusive gas separation, Front. Bioeng. Biotechnol. 10 (2022), https://doi.org/10.3389/fbioe.2022.861950, 861950.
[29] V. Galstyan, A. D'Arco, M. Di Fabrizio, N. Poli, S. Lupi, E. Comini, Detection of volatile organic compounds: from chemical gas sensors to terahertz spectroscopy, Rev. Anal. Chem. 40 (2021) 33–57, https://doi.org/10.1515/revac-2021-0127.
[30] G. Kavitha, K.T. Aru, P. Babu, Enhanced acetone gas sensing behavior of n-ZnO/p-NiO nanostructures, J. Mater. Sci. Mater. Electron. 29 (2018) 6666–6671, https://doi.org/10.1007/s10854-018-8652-9.
[31] R. Zhang, L. Lu, Y. Chang, M. Liu, Gas sensing based on metal-organic frameworks: concepts, functions, and developments, J. Hazard. Mater. 429 (2022) 128321, https://doi.org/10.1016/j.jhazmat.2022.128321.
[32] E. Manikandan, J. Kennedy, G. Kavitha, K. Kaviyarasu, M. Maaza, B.K. Panigrahi, U.K. Mudali, Hybrid nanostructured thin-films by PLD for enhanced field emission performance for radiation micro-nano dosimetry applications, J. Alloys Compd. 647 (2015) 141–145, https://doi.org/10.1016/j.jallcom.2015.06.102.
[33] K. Kaviyarasu, E. Manikandan, J. Kennedy, M. Maaza, Synthesis and analytical applications of photoluminescent carbon nanosheet by exfoliation of graphite

oxide without purification, J. Mater. Sci. Mater. Electron. 27 (2016) 13080–13085, https://doi.org/10.1007/s10854-016-5451-z.
[34] J. Kennedy, F. Fanga, J. Futter, J. Leveneur, P.P. Murmua, G.N. Paninc, T.W. Kang, E. Manikandan, Synthesis and enhanced field emission of zinc oxide incorporated carbon nanotubes, Diam. Relat. Mater. 71 (2017) 79–84, https://doi.org/10.1016/j.diamond.2016.12.007.
[35] E. Manikandan, V. Murugan, G. Kavitha, P. Babu, M. Maaza, Nanoflower rod wire-like structures of dual metal (Al and Cr) doped ZnO thin films: structural, optical and electronic properties, Mater. Lett. 131 (2014) 225–228, https://doi.org/10.1016/j.matlet.2014.06.008.
[36] E. Manikandan, G. Kavithac, J. Kennedy, Epitaxial zinc oxide, graphene oxide composite thin-films by laser technique for micro-Raman and enhanced field emission study, Ceram. Int. 40 (2014) 16065–16070, https://doi.org/10.1016/j.ceramint.2014.07.129.
[37] K.T. Arul, E. Manikandan, R. Ladchumananandasivam, M. Maaza, Novel polyvinyl alcohol polymer based nanostructure with ferrites co-doped with nickel and cobalt ions for magneto-sensor application, Polym. Int. 65 (2016) 1482–1485, https://doi.org/10.1002/pi.5242.
[38] X.-Q. Ma, H.-P. Xiao, Y. Chen, Q.-S. Lai, X.-X. Li, S.-T. Zheng, Polyoxometalate-based macrocycles and their assembly, Coord. Chem. Rev. 510 (2024) 215818, https://doi.org/10.1016/j.ccr.2024.215818.
[39] K. Arora, N. Chaudhary, S.C. Sahoo, K. Ghosh, P.P. Neelakandan, An ultrasensitive NO_2 sensor based on lightweight flexible organic single crystals, Chem. Eng. J. 502 (2024) 157905, https://doi.org/10.1016/j.cej.2024.157905.
[40] H.A.A.A. El-Wahab, A.K. Kamdy, C. Schulzke, T. Aboul-Fadl, W.S. Qayed, Crystal structure and quantum chemical calculations of (E)1-benzyl-3-((4 methoxyphenyl) imino)-5-methylindolin-2-one, J. Heterocycl. Chem. 58 (2021) 1601–1609, https://doi.org/10.1002/jhet.4284.
[41] M.K.R. Kandula, M. Gundluru, B.R. Nemallapudi, S. Gundala, P. Kotha, G. V. Zyryanov, S. Chadive, S.R. Cirandur, Synthesis, antioxidant activity, and α-glucosidase enzyme inhibition of α-aminophosphonate derivatives bearing piperazine-1,2,3-triazole moiety, J. Heterocycl. Chem. 58 (2021) 172–181, https://doi.org/10.1002/jhet.4157.
[42] E. Halay, I. Capan, R. Capan, E. Ay, Y. Acikbas, Heterocyclic-based Schiff base material designed as optochemical sensor for the sensitive detection of chlorinated solvent vapours, Res. Chem. Intermed. 50 (2024) 4579–4593, https://doi.org/10.1007/s11164-024-05359-6.
[43] L. Seifi, A. Torabian, H. Kazemian, G.N. Bidhendi, A.A. Azimi, F. Farhadi, S. Nazmara, Kinetic study of BTEX removal using granulated surfactant-modified natural zeolites nanoparticles, Water, Air, Soil Pollut. 219 (2011) 443–457, https://doi.org/10.1007/s11270-010-0719-z.
[44] M. Özacara, I.A. Sengil, A kinetic study of metal complex dye sorption onto pine sawdust, Process Biochem. 40 (2005) 565–572, https://doi.org/10.1016/j.procbio.2004.01.032.
[45] J. Wang, X. Guo, Adsorption kinetic models: physical meanings, applications, and solving methods, J. Hazard. Mater. 390 (2020) 122156, https://doi.org/10.1016/j.jhazmat.2020.122156.
[46] R. Capan, İ. Capan, F. Davis, A new approach for the adsorption kinetics using surface plasmon resonance results, Sens. Actuators, B 394 (2023) 134463, https://doi.org/10.1016/j.snb.2023.134463.
[47] Ş. Altın, F. Dumludag, Ç. Oruç, A. Altındal, Influence of humidity on kinetics of xylene adsorption onto ball-type hexanuclear metallophthalocyanine thin film, Microelectron. Eng. 134 (2015) 7–13, https://doi.org/10.1016/j.mee.2015.01.009.
[48] F.C. Wua, R.L. Tseng, R.S. Juang, Characteristics of Elovich equation used for the analysis of adsorption kinetics in dye-chitosan systems, Chem. Eng. J. 150 (2009) 366–373, https://doi.org/10.1016/j.cej.2009.01.014.
[49] M. Pişkin, N. Can, Z. Odabas, A. Altındal, Toluene vapor sensing characteristics of novel copper(II), indium(III), mono-lutetium(III) and tin(IV) phthalocyanines substituted with 2,6-dimethoxyphenoxy bioactive moieties, J. Porphyr. Phthalocyanines 22 (2018) 1–9, https://doi.org/10.1142/S1088424617500900.
[50] K. Triyana, A. Rianjanu, D.B. Nugroho, A.H. As'ari, A. Kusumaatmaja, R. Roto, R. Suryana, H.S. Wasisto, A highly sensitive safrole sensor based on polyvinyl acetate (PVAc) nanofiber-coated QCM, Sci. Rep. 9 (2019) 15407, https://doi.org/10.1038/s41598-019-51851-0.
[51] A. Rianjanu, K. Triyana, D.B. Nugroho, A. Kusumaatmaja, R. Roto, Electrospun polyvinyl acetate nanofiber modified quartz crystal microbalance for detection of primary alcohol vapor, Sens. Actuators, A A. 301 (2020) 111742, https://doi.org/10.1016/j.sna.2019.111742.
[52] R. Capan, I. Capan, M. Bayrakci, Quartz crystal microbalance modified with rhodamine-polyacrylonitrile nanofibers for acetone vapor sensing, Mater. Sci. Eng. B 322 (2025) 118581, https://doi.org/10.1016/j.mseb.2025.118581.
[53] E. Haghighi, S. Zeinali, Formaldehyde detection using quartz crystal microbalance (QCM) nanosensor coated by nanoporous MIL-101(Cr) film, Microporous Mesoporous Mater. 300 (2020) 110065, https://doi.org/10.1016/j.micromeso.2020.110065.
[54] Y. Acikbas, R. Capan, M. Erdogan, N. Cankaya, C. Soykan, Characterization of N-cyclohexylmethacrylamide LB thin films for room temperature vapor sensor application, J. Macromol. Sci., Pure Appl. Chem. 53 (2016) 132–139, https://doi.org/10.1080/10601325.2016.1132907.
[55] S. Şen, F. Cömert Önder, R. Çapan, M. Ay, A room temperature acetone sensor based on synthesized tetranitro-oxacalix[4]arenes: thin film fabrication and sensing properties, Sens. Actuators, A 315 (2020) 112308, https://doi.org/10.1016/j.sna.2020.112308.
[56] C. Ozkaya Erdogan, R. Capan, Y. Acikbas, M. Ozmen, M. Bayrakci, Sensor application of pyridine modified calix[4]arene Langmuir-Blodgett thin film, Optik 265 (2022) 169492, https://doi.org/10.1016/j.ijleo.2022.169492.
[57] M.G. Manera, R. Rella, Improved gas sensing performances in SPR sensors by transducers activation, Sens. Actuators, B 179 (2013) 175–186, https://doi.org/10.1016/j.snb.2012.10.028.
[58] C. He, L. Liu, S. Korposh, R. Correia, S.P. Morgan, Volatile organic compound vapour measurements using a localised surface plasmon resonance optical fibre sensor decorated with a metal-organic framework, Sensors 21 (2021) 1420, https://doi.org/10.3390/s21041420.
[59] F. Usman, J.O. Dennis, E.M. Mkawi, Y. Al-Hadeethi, F. Meriaudeau, Y.W. Fen, A. R. Sadrolhosseini, T.L. Ferrell, A. Alsadig, A. Sulieman, Acetone vapor-sensing properties of chitosan-polyethylene glycol using surface plasmon resonance technique, Polymers 12 (2020) 2586, https://doi.org/10.3390/polym12112586.
[60] Y. Acikbas, G. Dogan, M. Erdoğan, R. Çapan, C. Soykan, Organic vapor sensing properties of copolymer Langmuir-Blodgett thin film sensors, J. Macromol. Sci., Pure Appl. Chem. 53 (2016) 470–474, https://doi.org/10.1080/10601325.2016.1189279.
[61] K. Büyükkabasakal, S.C. Acikbas, A. Deniz, Y. Acikbas, R. Capan, M. Erdogan, Chemical sensor properties and mathematical modeling of graphene oxide Langmuir-Blodgett thin films, IEEE Sens. J. 19 (2019) 9097–9104, https://doi.org/10.1109/JSEN.2019.2926367.
[62] Y. Acikbas, R. Capan, M. Erdogan, F. Yukruk, Thin film characterization and vapor sensing properties of a novel perylenediimide material, Sens. Actuators, B 160 (2011) 65–71, https://doi.org/10.1016/j.snb.2011.07.013.
[63] P. Sun, Y. Jiang, G. Xie, J. Yu, X. Du, J. Hu, Synthesis and sensitive properties of poly-(bistriethylphosphine)-platinum-diethynylbenzene for organic vapor detection, J. Appl. Polym. Sci. 116 (2010) 562–567, https://doi.org/10.1002/app.31506.
[64] L.G. Xu, X. Hu, Y.T. Lim, V.S. Subramanian, Organic vapor adsorption behavior of poly(3-butoxythiophene) LB films on quartz crystal microbalance, Thin Solid Films 417 (2002) 90–94, https://doi.org/10.1016/S0040-6090(02)00634-X.
[65] R. Çapan, D. Öğrence, H. Namli, Schiff base thin film materials for chloroform vapor detection, ChemistrySelect 10 (2025) e03439, https://doi.org/10.1002/slct.202503439.
[66] S. Wang, L. Huang, Y. Zhang, L. Li, X. Lu, A mini-review on the modeling of volatile organic compound adsorption in activated carbons: equilibrium, dynamics, and heat effects, Chin. J. Chem. Eng. 31 (2021) 153–163, https://doi.org/10.1016/j.cjche.2020.11.018.
[67] L. Largitte, R. Pasquier, A review of the kinetics adsorption models and their application to the adsorption of lead by an activated carbon, Chem. Eng. Res. Des. 109 (2016) 495–504, https://doi.org/10.1016/j.cherd.2016.02.006.
[68] A. Yazıcı, N. Dalbul, A. Altındal, B. Salih, Ö. Bekaroğlu, Ethanol sensing property of novel phthalocyanines substituted with 3,4-dihydroxy-3-cyclobuten-1,2-dione, Sens. Actuators, B 202 (2014) 14–22, https://doi.org/10.1016/j.snb.2014.05.056.